Journal of Organometallic Chemistry, 332 (1987) 345–360
Elsevier Sequoia S.A., Lausanne – Printed in The Netherlands

Mechanistic studies on the carbonylation of amidohydrocarbylnickel derivatives

Michael D. Fryzuk* *, Patricia A. MacNeil and Steven J. Rettig **

Department of Chemistry, University of British Columbia, 2036 Main Mall, Vancouver, B.C. V6T 1Y6 (Canada)

(Received March 11th, 1987)

Abstract

The amidohydrocarbylnickel(II) complexes Ni(R)[N($SiMe_2CH_2PR'_2$)$_2$] (R′ = Ph, R = CH_3, $CH{=}CH_2$, C_6H_5, and C_6H_4-*p*-NMe_2; R′ = Me, R = C_6H_5) react with carbon monoxide to generate nickel(0) derivatives of the formula Ni(CO)$_2$[RC=N($SiMe_2CH_2PR'_2$)OSi$Me_2CH_2PR'_2$]. An intermediate in this process is the acylnickel species Ni(COR)[N($SiMe_2CH_2PR'_2$)$_2$] which has been isolated for all but the vinylnickel derivative; in this last case, addition of one equiv. of CO generates a 50% conversion to Ni(CO)[(η^2-CH_2=CH)C=N($SiMe_2CH_2PPh_2$)OSi$Me_2CH_2PPh_2$]. Addition of unlabelled CO to the specifically labelled benzoyl complex Ni(^{13}COC$_6$H$_5$)[N($SiMe_2CH_2PPh_2$)$_2$] produces Ni(CO)$_2$[$C_6H_5{}^{13}$C=N($SiMe_2CH_2PR'_2$)OSi$Me_2CH_2PR'_2$] as the only product establishing that no CO insertion into the Ni amide bond is occurring. Kinetic measurements are consistent with an associative pathway for the reductive elimination of the acyl and amide ligands. The X-ray crystal structure of Ni(COC_6H_5)[N($SiMe_2CH_2PPh_2$)$_2$] is reported and shows that the acyl unit is perpendicular to the square-plane of the complex; the Ni–C bond distance of 1.878 Å is typical of a single bond.

Introduction

In the process of investigating the carbonylation chemistry of a series of square-planar hydrocarbylnickel(II) complexes of the formula Ni(R)[N($SiMe_2CH_2PPh_2$)$_2$], where R = methyl, vinyl or phenyl, we discovered [1,2] an unusual transformation-rearrangement apparently involving the formation of a carbon–nitrogen bond by a reductive elimination sequence. Although reductive elimination reactions to generate C–C, C–H and H–H bonds have been extensively studied [3–5], little is known about the analogous sequence to generate C–N bonds [6].

* Fellow of the Alfred P. Sloan Foundation (1984–1987).
** Experimental Officer: UBC Crystal Structure Service.

0022-328X/87/$03.50

Addition of carbon monoxide (1 atm) to the nickel(II) complexes **1** results in a formal reduction of the metal centre and rearrangement of the ancillary tridentate ligand to generate the dicarbonylnickel(0) derivatives **2** as shown in eq. 1.

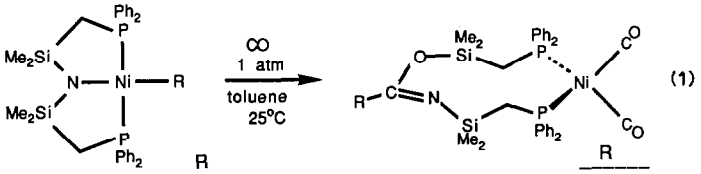

(1)

	R
1a	Me
1b	$CH=CH_2$
1c	Ph

	R
2a	Me
2b	$CH=CH_2$
2c	Ph

The formation of these nickel(0) species $Ni(CO)_2[R\overline{C=N(SiMe_2CH_2PPh_2)}OSiMe_2CH_2PPh_2]$ (**2a–2c**), can result from initial migratory insertion of CO into either the nickel–carbon bond of the hydrocarbyl ligand or the nickel–nitrogen bond of the amido ligand [7] followed by reductive elimination and a N,O-silatropic rearrangement [2]. In this paper we present the results of a mechanistic study of this intriguing involvement of the ancillary ligand in the reaction of carbon monoxide with hydrocarbylnickel(II) complexes. Also included in this work is the first single crystal X-ray analysis of a benzoylnickel(II) derivative.

Experimental

General procedures. The preparation and manipulation of all compounds were carried out using standard techniques and equipment for handling air- and moisture-sensitive materials as previously described [8]. The syntheses of $Ni(R)[N(SiMe_2CH_2PPh_2)_2]$ ($R = CH_3$, **1a**; $R = CH{=}CH_2$, **1b**; $R = C_6H_5$, **1c**) [8], $NiCl_2 \cdot DME$ (DME = 1,2-dimethoxyethane) [9], and $LiN(SiMe_2CH_2PMe_2)_2$ [10] were by standard literature procedures. All Grignard reagents were freshly prepared in tetrahydrofuran (THF) by standard methods and titrated immediately before use with 0.10 *M* HCl. All NMR spectra were recorded in C_6D_6 (Aldrich; dried over activated 3 Å sieves) unless otherwise indicated. Chemical shifts are in ppm with the coupling constants expressed in Hz. ^1H NMR spectra are referenced to C_6D_5H at 7.15 ppm, while $^{31}P\{^1H\}$ NMR chemical shifts are referenced to external $P(OMe)_3$ set at +141.0 ppm.

$NiCl[N(SiMe_2CH_2PMe_2)_2]$. To a suspension of $NiCl_2 \cdot DME$ (0.46 g, 2.0 mmol) in toluene (60 ml) at 0 °C was added a solution of $LiN(SiMe_2CH_2PMe_2)_2$ (0.57 g, 2.0 mmol) in toluene (10 ml). The solution rapidly became cherry red in colour. The reaction mixture was stirred at 0 °C for 0.5 h and then at room temperature for an additional 0.5 h. Removal of the solvent yielded an orange-brown solid which was extracted with hexanes (15–20 ml), filtered through celite and the filtrate reduced in volume (to approx. 3–5 ml). Upon cooling to −30 °C, dark green-red needles precipitated out of solution. These were washed with cold (−30 °C) hexanes (2 ml) and dried under vacuum. Yield: 0.54 g (72%). $^{31}P\{^1H\}$ NMR: −5.95 (s). ^1H NMR: $Si(CH_3)_2$, 0.27 (s); PCH_2Si, 0.47 (t, $J_{app} = 6.0$); $P(CH_3)_2$, 1.12 (t, $J_{app} = 4.2$). Anal. Found: C, 32.23; H, 7.60; N, 3.55. $C_{10}H_{28}ClNNiP_2Si_2$ calcd.: C, 32.04; H, 7.48; N, 3.74%.

$Ni(C_6H_5)[N(SiMe_2CH_2PMe_2)_2]$. To a solution of $NiCl[N(SiMe_2CH_2PMe_2)_2]$ (0.37 g, 1.0 mmol) in diethyl ether (Et_2O, 50 ml) at 0 °C, was slowly added a freshly prepared solution of PhMgCl in THF (1.0 ml, 1.0 *M*, 1.0 mmol). The resultant pale-yellow solution was stirred at 0 °C for 0.5 h then pumped to dryness. The mixture was extracted with hexanes, filtered and crystallized from minimum hexanes at −30 °C to give gold-coloured needles. Yield: 0.33 g (80%). $^{31}P\{^1H\}$ NMR: −3.68 (s). ^1H NMR: $Si(CH_3)_2$, 0.36 (s); PCH_2Si, 0.73 (t, $J_{app} = 5.1$); $P(CH_3)_2$, 0.76 (t, $J_{app} = 4.2$); C_6H_5, 6.98, 7.05, 7.38, 7.45 (m). Anal. Found: C, 46.22; H, 7.80; N, 3.20. $C_{16}H_{33}NNiP_2Si_2$ calcd.: C, 46.15; H, 7.93; N, 3.36%.

$Ni(COC_6H_5)[N(SiMe_2CH_2PMe_2)_2]$. A solution of $Ni(C_6H_5)[N(SiMe_2CH_2PMe_2)_2]$ (0.21 g, 0.5 mmol) in toluene (20 ml) was stirred under 1 atm CO for 1 h at room temperature. The initially yellow solution became clear orange in colour during this time. The excess CO and solvent were removed in vacuo to yield yellow-orange crystals of the product. Recrystallization from hexanes at −30 °C gave orange needles which were washed with a small amount of cold hexanes and dried under vacuum. Yield: 0.19 g (90%), $^{31}P\{^1H\}$ NMR: −5.42 (s). ^1H NMR: $Si(CH_3)_2$, 0.33, 0.38 (s); PCH_2Si, 0.68 (m); $P(CH_3)_2$, 0.66 (t, $J_{app} = 3.0$), 1.03 (t, $J_{app} = 3.8$); COC_6H_5, 7.20, 8.43 (m). Anal. Found: C, 46.25; H, 7.60; N, 3.05. $C_{17}H_{33}NNiOP_2Si_2$ calcd.: C, 45.96; H, 7.49; N, 3.15%. IR (KBr, cm^{-1}) ν(COPh) 1590 (s).

$Ni(CO)_2[(C_6H_5)\overline{C=N(SiMe_2CH_2PMe_2)}OSiMe_2CH_2PMe_2]$. A solution of $Ni(C_6H_5)[N(SiMe_2CH_2PMe_2)_2]$ (0.11 g, 0.25 mmol) in toluene (20 ml) was stirred under 1 atm CO for one day. The solution gradually faded in colour from a deep-yellow to a pale-yellow. The solvent was removed in vacuo and the resultant oil taken up in hexanes (2 ml) and cooled to −30 °C; off-white crystals were obtained. Alternatively, this nickel(0) complex can be prepared in an identical fashion using the benzoyl complex $Ni(COC_6H_5)[N(SiMe_2CH_2PMe_2)_2]$. Yield: 0.10 g (79%). $^{31}P\{^1H\}$ NMR: −14.5 (s, br). ^1H NMR: $Si(CH_3)_2$, 0.21, 0.29 (s, br); PCH_2Si, 0.99 (m, br); $P(CH_3)_2$, 1.24 (m, br); $N{=}CC_6H_5$, 7.08, 7.67 (m). Anal. Found: C, 45.87; H, 6.70; N, 2.87. $C_{19}H_{33}NNiO_3P_2Si_2$ calcd.: C, 45.61; H, 6.65; N, 2.80%. IR (KBr, cm^{-1}): ν(CO) 1995, 1935 (vs); ν(C=N) 1700 (s).

$Ni(COCH_3)[N(SiMe_2CH_2PPh_2)_2]$. Carbon monoxide (1.1 equiv., 25 ml, 0.2 atm) was added via a calibrated gas bulb to a solution of $Ni(CH_3)[N(SiMe_2CH_2PPh_2)_2]$ (0.12 g, 0.20 mmol) in toluene (20 ml) and stirred at room temperature for 5 h; no apparent colour change took place during this period. The solvent was removed under vacuum and the product recrystallized from toluene/hexanes. Yield: 0.10 g (78%). $^{31}P\{^1H\}$ NMR: 15.6 (s). ^1H NMR (25 °C): $Si(CH_3)_2$, 0.30 (br s); PCH_2Si, 1.82 (br t); $COCH_3$, 1.71 (t, $^4J(P) = 1.2$); $P(C_6H_5)_2$, 7.25 (m, *para/meta*), 8.0 (m, *ortho*). Anal. Found: C, 61.06; H, 6.20; N, 2.14; $C_{32}H_{39}NNiOP_2Si_2$ calcd.: C, 60.95; H, 6.19; N, 2.22%. IR (KBr, cm^{-1}): ν(COMe) 1615 (s). The reaction of $Ni(CH_3)[N(SiMe_2CH_2PPh_2)_2]$ with carbon monoxide was also monitored at −80 °C in a 5 mm NMR tube as follows: 20 mg of **1a** was dissolved in 0.4 ml of toluene-d_8 in an NMR tube attached to a ground-glass joint which was in turn attached to Kontes needle valve and cooled to −80 °C. CO was admitted (approx. 700 mmHg) and the tube sealed with a torch. The sealed NMR tube was transferred to the precooled probe in the NMR and spectra taken as a function of time.

$Ni(COC_6H_5)[N(SiMe_2CH_2PPh_2)_2]$. A solution of $Ni(C_6H_5)[N(SiMe_2CH_2$-

$PPh_2)_2$] (0.06 g, 0.10 mmol) in toluene (10 ml) was stirred under 1 atm CO for one hour. During this period, the original gold-coloured solution became clear orange. The solvent was removed in vacuo and the product recrystallized as orange blocks from toluene/hexanes at −30 °C. Yield: 0.48 g (70%), m.p. 163–165 °C. $^{31}P\{^1H\}$ NMR: 15.9 (s). ^1H NMR: $Si(CH_3)_2$, −0.01, 0.45 (s); PCH_2Si, 1.54 (dt, $^2J(H) = 13.7$, $J_{app} = 6.5$), 1.80 (dt, $J_{app} = 5.0$); $P(C_6H_5)_2$, 6.75, 7.12 (m, *para/meta*), 7.90, 8.21 (m, *ortho*); COC_6H_5, 7.28 (m). Anal. Found: C, 64.31; H, 5.98; N, 2.16. $C_{37}H_{41}NNiOP_2Si_2$ calcd.: 64.16; H, 5.92; N, 2.02%. IR (KBr, cm^{-1}): ν(COPh) 1602 (s). The ^{13}C-labelled material, $Ni(^{13}COC_6H_5)N(SiMe_2CH_2PPh_2)_2]$, was prepared in an identical fashion using ^{13}CO (Merck, Sharpe and Dohme: 92% enriched with ^{13}C).

$Ni(CO\text{-}p\text{-}C_6H_4NMe_2)[N(SiMe_2CH_2PPh_2)_2]$. The Grignard reagent *p*-$Me_2NC_6H_4MgBr$, prepared from *p*-$Me_2NC_6H_4Br$ and Mg in refluxing THF, was added to $NiCl[N(SiMe_2CH_2PPh_2)_2]$ to generate the corresponding arylnickel(II) derivative analogous to that previously described [8]. Anal. Found: C, 64.80; H, 6.68; N, 3.90. $C_{38}H_{46}N_2NiP_2Si_2$ calcd.: C, 64.50; H, 6.55; N, 3.96%. This material was subjected to 1 atm CO for one hour as described above for the benzoylnickel(II) derivative to generate orange crystals of $Ni(CO\text{-}p\text{-}C_6H_4NMe_2)[N(SiMe_2CH_2PPh_2)_2]$ in 80% yield. ^1H NMR: $Si(CH_3)_2$, 0.00, 0.43 (s); PCH_2Si, 1.60 (dt, $^2J = 14.0$, $J_{app} = 7.0$), 1.79 (dt, $J_{app} = 6.0$); $P(C_6H_5)_2$, 6.88, 7.15 (m, *para/meta*), 7.43, 8.21 (m, *ortho*); $COC_6H_4\text{-}p\text{-}NMe_2$, 7.97, 6.10 (d, $^3J_{vic} = 8.0$); $N(CH_3)_2$, 2.31 (s). Anal. Found: C, 63.82; H, 6.44; N, 3.90. $C_{39}H_{46}N_2NiOP_2Si_2$ calcd.: C, 63.68; H, 6.30; N, 3.81%.

Hydrolysis of $Ni(CO)_2[(C_6H_5)^{13}\overline{C=N(SiMe_2CH_2PPh_2)}OSiMe_2CH_2PPh_2]$. The selectively ^{13}C-labelled complex $Ni(^{13}COC_6H_5)[N(SiMe_2CH_2PPh_2)_2]$ was prepared as described above and subjected to unlabelled CO to generate the nickel(0) derivative. The hydrolysis was carried out by dissolving the nickel(0) complex (10 mg, 0.013 mmol) in THF (5 ml) and adding degassed water (2.5 μl, 0.014 mmol). The mixture was stirred at room temperature for three days. After this time, the volatiles were removed in vacuo and the residue sublimed onto a water-cooled probe. Benzamide was obtained as a fine, white powder and analyzed by low-resolution mass spectrocopy as being 94 ± 2% ^{13}C-labelled.

Kinetic analyses. Kinetic runs were carried out in a 25 ml round-bottomed flask attached directly to a 10 mm quartz UV cell; the entire apparatus has an approximately 50 ml total volume and was attached to a vacuum line by means of a ground-glass joint equipped with a needle valve inlet. For each run, 10 ml of a 3×10^{-4} *M* solution of the appropriate nickel(II) complex (see Results and discussion) was loaded in the flask assembly, freeze-pumped-thawed several times, and placed under a measured CO pressure at 22.0 °C. The reaction mixture was stirred between spectral readings: 400 nm for **1b**; 400 nm for **3c**; 375 nm for **4**; 410 nm for **3d**. Plots of $\ln(A_\infty - A)$ vs. time were linear for at least two half-lives. All of these systems obey Beer's Law at the observed wavelengths over the concentration range studied. Plots of $k_{observed}$ vs. CO pressure indicated a first order dependence upon CO. Second-order rate constants were calculated using the literature value for the solubility of CO in toluene [11] after correcting for the vapor pressure of toluene at 22 °C ($p(C_7H_8)$ 2.6 cmHg).

X-Ray crystallographic analysis of $Ni(COC_6H_5)[N(SiMe_2CH_2PPh_2)_2]$. Crystallographic data appear in Table 1. Unit cell parameters were determined by least-

Table 1

Crystallographic data [a]

Compound	$Ni(COC_6H_5)[N(SiMe_2CH_2PPh_2)_2]$ (3c)
Formula	$C_{37}H_{41}NNiOP_2Si_2$
fw.	692.57
Crystal system	triclinic
Space group	$P\bar{1}$ [b]
a (Å)	10.8891(6)
b	11.3380(7)
c	16.1785(10)
α (deg)	104.359(4)
β	105.704(4)
γ	100.062(4)
V (Å^3)	1799.1(2)
Z	2
D_c (g/cm^3)	1.279
$F(000)$	728
μ(Cu-K_α) (cm^{-1})	24.9
Crystal dimensions (mm)	0.09×0.13×0.18
Transmission factors	0.384–0.703
Scan type	ω–2θ
Scan range (deg in ω)	0.75 + 0.15 tan θ
Scan speed (deg/min)	1.34–10.06
Data collected	$\pm h, -k, \pm l$
$2\theta_{max}$ (deg)	150
Unique reflections	7419
Reflections with $I \geq 3\sigma(I)$	5269
Number of variables	561
R	0.040
R_w	0.047
S	1.853
Mean Δ/σ (final cycle)	0.02
Max Δ/σ (final cycle)	0.24 [z for H(2a)]
Residual density (e/Å^3)	−0.85 to +0.26

[a] Temperature 22°C, Enraf–Nonius CAD4-F diffractometer, Cu-K_α radiation ($\lambda_{K\alpha 1}$ 1.540562, $\lambda_{K\alpha 2}$ 1.544390 Å), graphite monochromator, takeoff angle 2.7°, aperture (2.00 + tan θ)×4.0 mm at a distance of 173 mm from the crystal, scan range extended by 25% on both sides for background measurement, $\sigma^2(I) = S + 2B + [0.035(S-B)]^2$ (S = scan count, B = normalized background count), function minimized $\Sigma w(|F_o| - |F_c|)^2$ where $w = 1/\sigma^2(F)$, $R = \Sigma ||F_o| - |F_c|| / \Sigma |F_o|$, $R_w = (\Sigma w(|F_o| - |F_c|)^2 / \Sigma w|F_o|^2)^{1/2}$, $S = (\Sigma w(|F_o| - |F_c|)^2/(m-n))^{1/2}$. Values given for R, R_w, and S are based on those reflections with $I \geq 3\sigma(I)$. [b] Reduced cell.

squares on 2 sin θ/λ values for 25 reflections with 2θ 80–100°. The intensities of three standard reflections, measured every hour of X-ray exposure time during the data collection, showed only small random variations. The data were processed and corrected for absorption using the analytical method [12 *–14]; the range of the transmission factors appears in Table 1.

The centrosymmetric space group $P\bar{1}$ was suggested by both the E-statistics and by the Patterson function, from which the coordinates of the Ni, P, and Si atoms

* Reference number with asterisk indicates a note in the list of references.

Table 2

Final positional (fractional$\times 10^5$; O, N, and C$\times 10^4$, H$\times 10^3$) and isotropic thermal parameters ($U \times 10^3$ Å^2) with estimated standard deviations in parentheses

Atom	x	y	z	U_{eq}/U_{iso}
Ni	45448(4)	23040(4)	27179(2)	38
P(1)	47748(6)	8643(6)	33956(4)	41
P(2)	44365(6)	35614(6)	18781(4)	40
Si(1)	68317(7)	31641(7)	46139(5)	50
Si(2)	66137(7)	49842(7)	35613(5)	52
O	3024(2)	366(2)	1160(1)	56
N	6034(2)	3591(2)	3720(1)	45
C(1)	5651(3)	1704(3)	4580(2)	48
C(2)	5220(3)	5142(3)	2640(2)	51
C(3)	8427(3)	2807(5)	4579(3)	81
C(4)	7185(6)	4320(4)	5759(2)	85
C(5)	8091(4)	5077(5)	3190(3)	82
C(6)	7006(6)	6418(4)	4565(3)	91
C(7)	3024(2)	1169(2)	1823(2)	41
C(8)	3309(2)	−289(2)	3316(2)	46
C(9)	2942(3)	−1521(3)	2769(2)	63
C(10)	1756(4)	−2339(3)	2668(3)	79
C(11)	953(4)	−1917(4)	3124(3)	83
C(12)	1294(3)	−699(4)	3669(3)	80
C(13)	2468(3)	125(3)	3767(2)	62
C(14)	5807(2)	−110(2)	3016(2)	48
C(15)	5634(3)	−520(3)	2101(2)	65
C(16)	6370(4)	−1276(4)	1781(3)	84
C(17)	7305(4)	−1628(4)	2356(3)	82
C(18)	7487(4)	−1227(4)	3263(3)	82
C(19)	6759(3)	−468(3)	3599(2)	66
C(20)	2852(2)	3570(2)	1122(2)	44
C(21)	2405(3)	2889(3)	216(2)	60
C(22)	1167(3)	2823(4)	−331(2)	75
C(23)	366(3)	3451(4)	15(3)	74
C(24)	776(3)	4091(4)	905(3)	82
C(25)	2013(3)	4165(3)	1462(2)	65
C(26)	5410(2)	3256(3)	1130(2)	46
C(27)	5668(3)	2081(3)	914(2)	61
C(28)	6380(3)	1787(4)	333(2)	74
C(29)	6842(4)	2660(5)	−23(3)	84
C(30)	6612(4)	3823(5)	179(3)	91
C(31)	5887(3)	4127(4)	761(2)	69
C(32)	1711(2)	1288(2)	1931(2)	42
C(33)	1642(3)	2159(3)	2675(2)	55
C(34)	442(3)	2268(3)	2762(2)	69
C(35)	−705(3)	1512(4)	2101(3)	82
C(36)	−642(3)	642(4)	1364(3)	95
C(37)	557(3)	527(3)	1279(2)	66
H(1a)	607(3)	116(3)	491(2)	59(8)
H(1b)	502(3)	201(3)	479(2)	54(8)
H(2a)	538(3)	569(4)	232(2)	98(12)
H(2b)	459(3)	532(3)	290(2)	73(10)
H(3a)	909(4)	360(4)	461(3)	111(14)
H(3b)	838(4)	215(5)	407(3)	133(20)
H(3c)	888(4)	246(4)	505(3)	110(14)
H(4a)	786(5)	490(5)	587(3)	128(21)
H(4b)	733(5)	380(5)	627(4)	181(21)

Table 2 (continued)

Atom	x	y	z	U_{eq}/U_{iso}
H(4c)	643(5)	466(5)	579(3)	130(19)
H(5a)	806(4)	433(4)	272(3)	111(17)
H(5b)	823(4)	579(5)	289(3)	139(17)
H(5c)	880(4)	512(4)	361(3)	121(17)
H(6a)	789(4)	666(4)	498(3)	104(13)
H(6b)	707(4)	715(4)	442(3)	108(14)
H(6c)	643(5)	632(5)	490(3)	135(21)
H(9)	348(3)	−177(3)	250(2)	52(9)
H(10)	154(3)	−329(4)	224(2)	95(11)
H(11)	23(4)	−235(4)	305(2)	92(12)
H(12)	71(4)	−40(4)	399(3)	115(15)
H(13)	277(3)	102(3)	414(2)	78(10)
H(15)	490(3)	−37(3)	171(2)	72(9)
H(16)	615(4)	−156(4)	115(3)	127(17)
H(17)	781(3)	−218(3)	210(2)	76(10)
H(18)	804(4)	−135(4)	372(3)	98(12)
H(19)	683(3)	−23(3)	421(2)	61(8)
H(21)	295(3)	248(3)	−2(2)	84(11)
H(22)	89(3)	235(3)	−96(2)	82(11)
H(23)	−60(3)	339(3)	−38(2)	82(10)
H(24)	28(4)	444(4)	121(3)	101(13)
H(25)	231(3)	462(3)	205(2)	87(12)
H(27)	537(3)	145(3)	114(2)	82(11)
H(28)	657(5)	88(5)	14(3)	142(17)
H(29)	736(4)	245(4)	−41(3)	96(12)
H(30)	690(5)	454(5)	−2(3)	136(18)
H(31)	566(3)	485(4)	91(2)	82(12)
H(33)	251(3)	266(3)	316(2)	69(9)
H(34)	42(3)	296(3)	325(2)	82(10)
H(35)	−156(3)	173(3)	214(2)	86(11)
H(36)	−151(4)	15(4)	84(3)	121(14)
H(37)	70(4)	−8(4)	79(3)	102(13)

were determined. The coordinates of all remaining atoms, including hydrogen, were determined from subsequent difference maps. In the final stages of full-matrix least-squares refinement, the non-hydrogen atoms were refined with anisotropic thermal parameters and the hydrogen atoms with isotropic parameters. Neutral atom scattering factors for all atoms and anomalous scattering corrections for Ni, P, and Si were taken from ref. 15.

Final positional and isotropic [or equivalent isotropic, $U_{eq} = 1/3$ trace (diagonalized U)] thermal parameters are given in Table 2. Bond lengths and bond angles appear in Tables 3 and 4 respectively. Anisotropic thermal parameters, bond lengths and angles involving hydrogen atoms, torsion angles, and measured and calculated structure factor amplitudes (Tables S1–S5) are available from the authors as supplementary material.

Notes on the structure. The shortest intermolecular contact is H(23) · · · H(29) ($x-1$, y, z) 2.28(5) Å. There is an intermolecular hydrogen bond: C(28)–H(28) · · · O ($1-x$, $-y$, $-z$), H · · · O 2.42(5), C · · · O 3.271(4) Å, C–H · · · O 135(3)°. There are two intramolecular hydrogen bonds: C(15)–H(15) · · · O, H · · · O 2.38(3),

Table 3

Bond lengths (Å) with estimated standard deviations in parentheses

Bond	Length (Å)	Bond	Length (Å)
Ni–P(1)	2.1934(7)	C(12)–C(13)	1.390(4)
Ni–P(2)	2.1966(7)	C(14)–C(15)	1.385(4)
Ni–N	1.991(2)	C(14)–C(19)	1.392(4)
Ni–C(7)	1.878(2)	C(15)–C(16)	1.375(4)
P(1)–C(1)	1.810(3)	C(16)–C(17)	1.369(5)
P(1)–C(8)	1.831(2)	C(17)–C(18)	1.370(5)
P(1)–C(14)	1.825(3)	C(18)–C(19)	1.381(5)
P(2)–C(2)	1.806(3)	C(20)–C(21)	1.380(4)
P(2)–C(20)	1.828(2)	C(20)–C(25)	1.378(4)
P(2)–C(26)	1.824(2)	C(21)–C(22)	1.375(4)
Si(1)–N	1.700(2)	C(22)–C(23)	1.366(5)
Si(1)–C(1)	1.889(3)	C(23)–C(24)	1.349(5)
Si(1)–C(3)	1.863(4)	C(24)–C(25)	1.378(4)
Si(1)–C(4)	1.879(4)	C(26)–C(27)	1.389(4)
Si(2)–N	1.704(2)	C(26)–C(31)	1.372(4)
Si(2)–C(2)	1.887(3)	C(27)–C(28)	1.386(4)
Si(2)–C(5)	1.859(4)	C(28)–C(29)	1.353(6)
Si(2)–C(6)	1.880(4)	C(29)–C(30)	1.361(6)
O–C(7)	1.223(3)	C(30)–C(31)	1.402(5)
C(7)–C(32)	1.511(3)	C(32)–C(33)	1.384(4)
C(8)–C(9)	1.377(4)	C(32)–C(37)	1.375(3)
C(8)–C(13)	1.390(4)	C(33)–C(34)	1.374(4)
C(9)–C(10)	1.395(4)	C(34)–C(35)	1.373(4)
C(10)–C(11)	1.363(6)	C(35)–C(36)	1.373(5)
C(11)–C(12)	1.364(6)	C(36)–C(37)	1.374(4)

C···O, 3.289(4) Å, C–H···O 162(3)°; C(37)–H(37)···O, H···O 2.37(4), C···O, 2.779(4) Å, C–H···O 104(3)°. The mean plane defined by the atoms directly bonded to the nickel centre is slightly distorted from square-planar to tetrahedral with the following deviations: P(1), 0.134(1); P(2), 0.135(1); N, −0.127(2); C(7), −0.143(3); Ni, −0.0373(4) Å.

Results and discussion

Synthetic studies. When the reaction of the methylnickel(II) derivative **1a** with carbon monoxide (> 3 equiv.) is monitored by ^{1}H NMR spectroscopy at −80 °C, the species formed almost immediately upon exposure to CO is the acetylnickel(II) complex $Ni(COCH_3)[N(SiMe_2CH_2PPh_2)_2]$ (**3a**). Most noteworthy is the fact that, at −80 °C, the silylmethyl protons ($Si(CH_3)_2$) of **3a** appear as two broad singlets of equal intensity, a result of restricted rotation about the nickel–carbon bond of the acetyl ligand (vide infra). Over a period of approximately two hours at −80 °C, these signals gradually disappear and are replaced by one sharp silylmethyl resonance indicative of the dicarbonylnickel(0) product **2a**; no other species are detectable during this transformation. The acetyl complex **3a** can be isolated as orange crystals via reaction of the methyl derivative **1a** with slightly greater than one equivalent of CO at room temperature (eq. 2); the spectral parameters for the isolated complex are identical to those of the species initially observed at low

Table 4

Bond angles (deg) with estimated standard deviations in parentheses

Bonds	Angle (deg)	Bonds	Angle (deg)
P(1)–Ni–P(2)	170.56(3)	P(1)–C(8)–C(13)	118.4(2)
P(1)–Ni–N	91.70(6)	C(9)–C(8)–C(13)	118.4(3)
P(1)–Ni–C(7)	89.49(7)	C(8)–C(9)–C(10)	121.0(3)
P(2)–Ni–N	91.61(6)	C(9)–C(10)–C(11)	119.6(4)
P(2)–Ni–C(7)	88.12(7)	C(10)–C(11)–C(12)	120.5(3)
N–Ni–C(7)	174.17(10)	C(11)–C(12)–C(13)	120.2(4)
Ni–P(1)–C(1)	106.38(9)	C(8)–C(13)–C(12)	120.2(3)
Ni–P(1)–C(8)	119.58(8)	P(1)–C(14)–C(15)	118.6(2)
Ni–P(1)–C(14)	112.61(8)	P(1)–C(14)–C(19)	123.3(2)
C(1)–P(1)–C(8)	107.90(12)	C(15)–C(14)–C(19)	118.1(3)
C(1)–P(1)–C(14)	106.07(13)	C(14)–C(15)–C(16)	120.7(3)
C(8)–P(1)–C(14)	103.55(12)	C(15)–C(16)–C(17)	121.1(4)
Ni–P(2)–C(2)	106.51(10)	C(16)–C(17)–C(18)	118.8(3)
Ni–P(2)–C(20)	121.04(8)	C(17)–C(18)–C(19)	121.1(3)
Ni–P(2)–C(26)	110.72(9)	C(14)–C(19)–C(18)	120.2(3)
C(2)–P(2)–C(20)	108.08(12)	P(2)–C(20)–C(21)	121.5(2)
C(2)–P(2)–C(26)	106.19(14)	P(2)–C(20)–C(25)	120.4(2)
C(20)–P(2)–C(26)	103.43(11)	C(21)–C(20)–C(25)	117.9(3)
N–Si(1)–C(1)	105.34(11)	C(20)–C(21)–C(22)	120.9(3)
N–Si(1)–C(3)	114.3(2)	C(21)–C(22)–C(23)	120.2(3)
N–Si(1)–C(4)	115.5(2)	C(22)–C(23)–C(24)	119.5(3)
C(1)–Si(1)–C(3)	109.4(2)	C(23)–C(24)–C(25)	121.0(3)
C(1)–Si(1)–C(4)	105.2(2)	C(20)–C(25)–C(24)	120.5(3)
C(3)–Si(1)–C(4)	106.6(2)	P(2)–C(26)–C(27)	118.5(2)
N–Si(2)–C(2)	105.39(11)	P(2)–C(26)–C(31)	123.1(2)
N–Si(2)–C(5)	115.0(2)	C(27)–C(26)–C(31)	118.4(3)
N–Si(2)–C(6)	114.8(2)	C(26)–C(27)–C(28)	121.0(3)
C(2)–Si(2)–C(5)	107.9(2)	C(27)–C(28)–C(29)	119.7(4)
C(2)–Si(2)–C(6)	106.2(2)	C(28)–C(29)–C(30)	120.8(3)
C(5)–Si(2)–C(6)	107.0(3)	C(29)–C(30)–C(31)	120.0(4)
Ni–N–Si(1)	118.57(11)	C(26)–C(31)–C(30)	120.1(4)
Ni–N–Si(2)	118.06(11)	C(7)–C(32)–C(33)	121.3(2)
Si(1)–N–Si(2)	122.54(12)	C(7)–C(32)–C(37)	119.8(2)
P(1)–C(1)–Si(1)	105.92(13)	C(33)–C(32)–C(37)	118.9(2)
P(2)–C(2)–Si(2)	105.37(14)	C(32)–C(33)–C(34)	120.8(3)
Ni–C(7)–O	124.8(2)	C(33)–C(34)–C(35)	119.9(3)
Ni–C(7)–C(32)	116.8(2)	C(34)–C(35)–C(36)	119.6(3)
O–C(7)–C(32)	118.4(2)	C(35)–C(36)–C(37)	120.6(3)
P(1)–C(8)–C(9)	122.9(2)	C(32)–C(37)–C(36)	120.3(3)

temperature under excess CO. Although stable in the solid-state, **3a** is unstable in solution decomposing to a mixture of the starting methyl complex **1a** and the nickel(0) product **2a**.

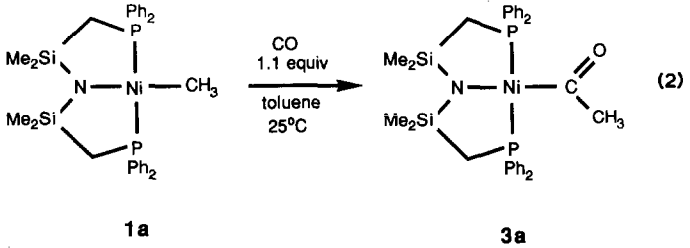

(2)

1a **3a**

The reaction of CO with the phenylnickel(II) derivative **1c** is considerably slower than for the analogous methyl complex **1a**; whereas production of the methylimidate species **2a** from **1a** is over in a few minutes (1 atm CO, 25 °C), under identical conditions the phenyl complex **1c** requires approximately two days to be converted to the corresponding phenylimidate derivative **2c**. The sluggish nature of the latter reaction has allowed for the interception of the benzoylnickel(II) complex, $Ni(COC_6H_5)[N(SiMe_2CH_2PPh_2)_2]$ (**3c**). Thus reaction of CO with **1c** for 1 h at room temperature (eq. 3) followed by recrystallization from toluene/hexanes at −30 °C produces pure **3c** as orange crystals of sufficient quality for single crystal X-ray analysis.

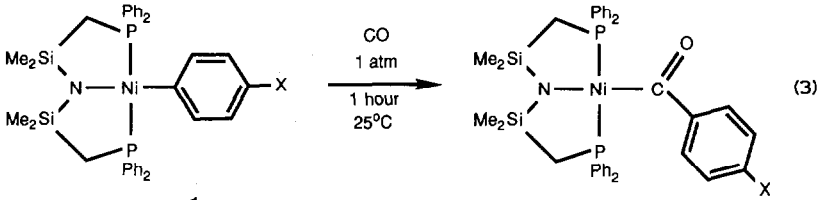

(3)

X = H **1c**

X = NMe_2 **1d**

X = H **3c**

X = NMe_2 **3d**

The results of the X-ray analysis for the benzoyl complex **3c** are shown in Fig. 1. In the solid state, the oxygen of the acyl carbonyl is oriented above and the benzoyl phenyl ring below the mean square-plane of the complex, thereby generating inequivalent environments for the tridentate ligand atom substituents. Interestingly, there is only a slight puckering in the ligand backbone of **3c** resulting in a C-envelope conformation for each chelate ring; this contrasts that observed [8] for $NiCl[N(SiMe_2CH_2PPh_2)_2]$ wherein the planar Si_2N unit is tilted by about 40 ° with respect to the square-plane of the coordination complex. The origin of the conformational difference in the ligand backbone can be traced to a longer Ni–N bond in **3c** (1.991 Å, Table 2) as compared to the chloro derivative (1.929 Å), which allows the two five-membered chelate rings of the former to expand and flatten; the Ni–P bond lengths for both complexes are not significantly different (i.e.: 2.1934 and 2.1966 Å for **3c**, and 2.212 and 2.201 Å for $NiCl[N(SiMe_2CH_2PPh_2)_2]$). The difference in the respective Ni–N bond lengths is a consequence of the fact that the acyl ligand has a greater *trans* influence [16] than a chloride ligand which results in destabilization and concomitant lengthening of the nickel–amide bond of **3c**. Although several benzoylnickel(II) complexes have been reported [17], no single crystal X-ray analysis has appeared in the literature to our knowledge. Other bond lengths (Table 2), bond and torsion angles (Tables 3 and 4) are not unusual.

That this structure persists in solution is supported by the ^1H NMR spectrum which has two sharp silylmethyl singlets and an AB quartet of virtual triplets for the methylene (PCH_2Si) protons. The silylmethyl singlets do broaden and coalesce above 100 °C, but the spectra are complicated by the fact that at these higher temperatures, deinsertion of CO to regenerate the starting phenylnickel(II) derivative **1c** also occurs. For the acetylnickel(II) complex **3a**, rotation about the Ni–C bond is more facile as evidenced by the fact that at room temperature, only one broad singlet for the silylmethyl protons is observed in the ^1H NMR spectrum. As has been previously mentioned, at lower temperatures, this rotation of the acetyl moiety can be frozen out.

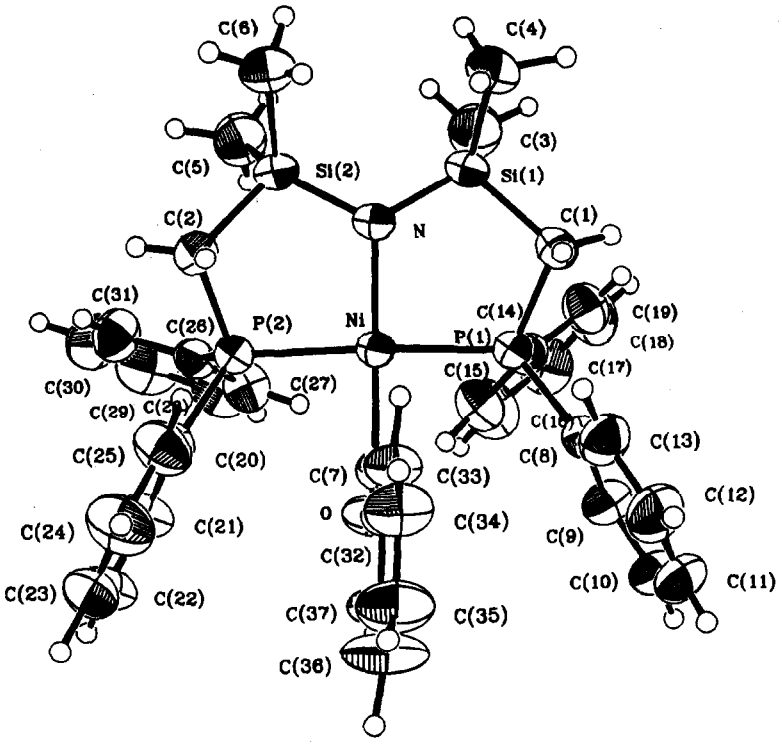

Fig. 1. Single crystal X-ray structure of $Ni(COC_6H_5)[N(SiMe_2CH_2PPh_2)_2]$ (**3c**) showing the atom numbering scheme.

Either of two possibilities may account for the observed restricted rotation of the benzoyl group of **3c** in solution. It is conceivable that the Ni–C bond possesses significant π-character owing to a contribution from canonical form **B**, a carbene resonance contribution. However, the crystallographic data do not support this

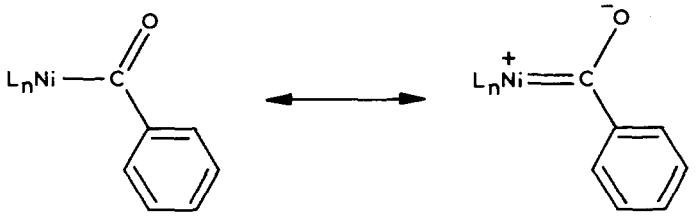

premise since the Ni–C bond length of 1.878 Å of **3c** is only slightly longer than that expected [18] for a square-planar Ni–C (sp^2) bond (sum of the covalent radii 1.867 Å); by comparison, a Ni–C bond length of 1.84 Å has been reported for the complexes *trans*-$Ni(COR)Cl(PMe_3)_2$ ($R = CH_3$ [19]; $R = CH_2SiMe_3$ [20]). In addition, the C–O bond length (1.223 Å) of the acyl carbonyl is typical of a double bond [21]. This lack of nickel–carbon double bond character is also supported by XPS studies [22] on a series of related nickel(II) complexes. The other possibility is that this restricted rotation is due entirely to steric interactions between the benzoyl

phenyl ring and the substituents on the phosphorus donors of the tridentate ligand. In fact, molecular models suggest that regardless of the size of the substituents on phosphorus, the benzoyl fragment is sterically encumbered and forced to adopt the observed conformation. To test this, we synthesized another benzoylnickel(II) complex having the smaller methyl substituents on the phosphorus donors; this is shown in eq. 4. The ^{1}H NMR spectrum of **4** shows inequivalent silylmethyl

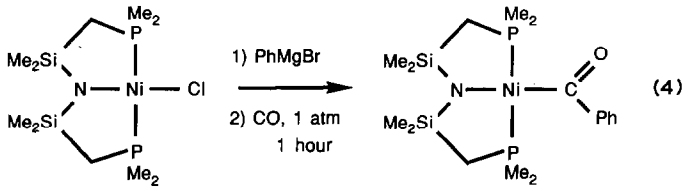

(4)

4

environments at room temperature indicative of restricted rotation on the NMR time scale. It follows therefore that reducing the size of the substituent on the acyl group should decrease the steric interaction with the phosphorus substituents and thereby allow free rotation; indeed, as already mentioned, the acetylnickel(II) complex **3a** displays facile rotation about the Ni–C bond at room temperature.

The formation of the benzoyl derivatives as described above can be extended to the *para*-dimethylaminophenyl complex Ni(C_6H_4-*p*-NMe_2)[$N(SiMe_2CH_2PPh_2)_2$] (**1d**); thus the aroylnickel derivative Ni(COC_6H_4-*p*-NMe_2)[$N(SiMe_2CH_2PPh_2)_2$] (**3d**) is obtained by stirring **1d** under 1 atm of CO for 1 h (eq. 3).

Attempts to prepare the acryloylnickel(II) complex Ni($COCH{=}CH_2$)[$N(SiMe_2CH_2PPh_2)_2$] from the vinylnickel(II) derivative **1b** by either of the routes used above to generate the acyl species **3a** and **3c**/**3d** were unsuccessful. Interestingly however, the reaction of **1b** with one equivalent of CO at room temperature yields an equimolar mixture of the starting material **1b** and the η^2-acrylimidic ester Ni(CO)[(η^2-$CH_2{=}CH)\overline{C{=}N(SiMe_2CH_2PPh_2)O}SiMe_2CH_2PPh_2$] (**5**) (eq. 5). This

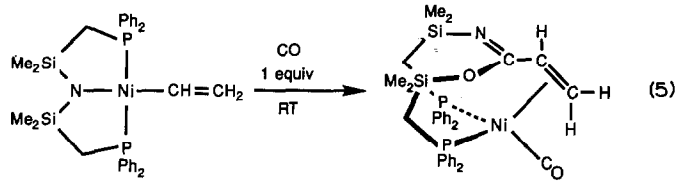

(5)

1b **5**

latter complex **5** has been prepared previously by the slow removal of CO under vacuum from the dicarbonyl derivative Ni$(CO)_2$[$CH_2{=}CH)\overline{C{=}N(SiMe_2CH_2PPh_2)O}$-$SiMe_2CH_2PPh_2$] (**2b**), and has been characterized crystallographically [2].

Both the acetylnickel(II) derivative **3a** and the aroylnickel(II) complexes **3c** and **3d** are converted to the respective nickel(0) products **2a**, **2c** and **2d** by further reaction with CO. To establish that these acyl species are bona fide intermediates, the following labelling study was performed. ^{13}C-enriched (92%) benzoylnickel(II) was isolated from the reaction of ^{13}CO with the phenylnickel(II) complex **1c** and then further subjected to unlabelled CO to generate the nickel(0) complex **2c**. To measure the extent of incorporation of the label in **2c** from **3c**, the product was

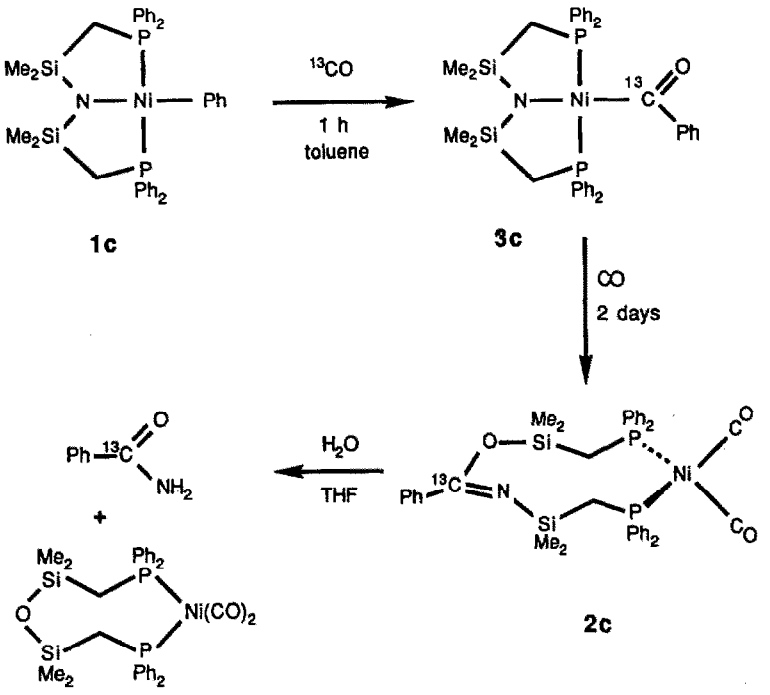

Scheme 1

hydrolyzed and the liberated benzamide analyzed by mass spectroscopy as outlined in Scheme 1. The isolated benzamide was $94 \pm 2\%$ ^{13}C-enriched which corresponds to no measurable loss of label during the transformation. A similar experiment was not attempted for the acetyl **3a** since it is unstable to CO loss. In any case, at least for the benzoyl derivatives, initial migratory insertion into the nickel–amide bond [7] is excluded.

Added carbon monoxide is the only ligand that induces reductive elimination of these acyl complexes. Addition of phosphines (e.g. PMe_3, $P(OMe)_3$ or $Me_2PCH_2CH_2PMe_2$), acetonitrile, diphenylacetylene or olefins (e.g. ethylene, 1,5-cyclooctadiene) to the benzoyl complex results in recovery of starting material in all cases.

Kinetic studies. At some point in the overall transformation of these acylnickel(II) derivatives into the dicarbonylnickel(0) complexes, a reductive elimination of the acyl and the amido ligands is required to generate the C–N bond in the disilylimidate backbone of the rearranged ligand. To gain some insight into this process, a cursory kinetic study was performed.

The reaction of CO with the benzoyl complex **3c** was monitored as a function of time by UV-VIS spectroscopy; this turned out to be the method of choice over ^{1}H or ^{31}P{^{1}H} NMR spectral analysis since the nickel(II) derivatives have a well-defined absorption in the 375–410 nm region (ϵ 700–800 l mol^{-1} cm^{-1}) whereas the nickel(0) products do not. Under 1 atm of CO (≥ 100 equiv.), the reaction is first order in **3c** with a pseudo-first-order rate constant of 2.67×10^{-5} s^{-1} at 22.0 °C. Variation of the CO pressure (0.5 to 1 atm) indicated a first-order dependence on

Table 5

Kinetic data for the carbonylation of $Ni(R)[N(SiMe_2CH_2PR'_2)_2]$ [a]

Entry	Complex	$10^5 k_{obsd}$ s^{-1} (p(CO) cmHg)	$10^3 k_2$ $l\ mol^{-1}\ s^{-1}$
1	$Ni(COC_6H_5)[N(SiMe_2CH_2PPh_2)_2]$ (**3c**)	2.56 (73.2)	3.53
2		1.73 (54.5)	
3		1.30 (34.9)	
4		2.71 (73.4) [b]	
5	$Ni(CO\text{-}p\text{-}C_6H_4NMe_2)[N(SiMe_2CH_2PPh_2)_2]$ (**3d**)	5.67 (68.9)	8.58
6		4.33 (49.5)	
7		2.90 (32.9)	
8	$Ni(COC_6H_5)[N(SiMe_2CH_2PMe_2)_2]$ (**4**)	1.88 (73.9)	2.67
9		1.30 (54.7)	
10	$Ni(CH{=}CH_2)[N(SiMe_2CH_2PPh_2)_2]$ (**1b**)	60.5 (68.9)	91.4
11		44.1 (50.9)	
12		28.9 (32.7)	

[a] All reactions performed in toluene at 22.0 °C. The solubility of CO in toluene is 0.0073 M at 22.0 °C at p(CO) 76.0 cmHg. The indicated CO partial pressures have been corrected for the partial pressure of toluene ($p(C_7H_8)$ 2.6 cmHg at 22 °C). [b] This run performed in the presence of 10 equiv. PMe_3.

CO; the second-order rate constant is calculated to be 3.53×10^{-3} l mol^{-1} s^{-1}. This rate is not affected by added PMe_3 (10 equiv., entry 4 in Table 5). Similar analyses were performed with the *para*-dimethylaminobenzoyl complex **3d** and the derivative **4** having methyl substituents at phosphorus; the results are shown in Table 5.

Although the acyl complex derived from the nickel vinyl starting material **1b** was not accessible (see eq. 5), we discovered that **1b** gave pseudo-first-order kinetics with a first-order dependence on CO partial pressure analogous to the behaviour of the isolated acyl derivatives; the second-order rate constant was found to be 91.4×10^{-3} l mol^{-1} s^{-1} (Table 5). Attempts to extend this to the methylnickel derivative **1a** were unsuccessful since no clean pseudo order-rate law was apparent.

The simple rate equation of the type $-d[Ni^{II}]/dt = k_2[Ni^{II}][CO]$ indicated from this study, is not particularly revealing. A mechanism which is reasonable for this process is shown in Scheme 2. It is assumed that the initial CO insertion step (k_1) to generate the acyl is sufficiently fast and irreversible (at least for the arylnickel(II) derivatives) that the observed rate law corresponds to the subsequent transformation of the nickel acyl **3**. Three possibilities exist for the rate determining step: (i) CO binding to the acyl **3** to generate the five-coordinate species **6**, (ii) rearrangement of the square-pyramidal isomer **6** to the corresponding isomer with the acyl and the amido ligand *cis* disposed as in **6'**, or (iii) reductive elimination of the acyl and amide ligands from the five-coordinate intermediate. As no build-up of any intermediates is observed by low temperature ^1H or $^{31}P\{^1H\}$ NMR spectroscopy, it is not possible to distinguish among the above paths.

The kinetic data clearly indicate that a five-coordinate nickel(II) species is involved as an intermediate; this is in agreement with other work on C–C [3,23] and C–O [24] bond reductive elimination sequences at nickel(II). However, there are some important aspects that should be pointed out: (i) in the study [24] of carbon–oxygen bond formation, reductive elimination from the five-coordinate nickel(II) intermediate was shown to be rate determining, and (ii) formation of both

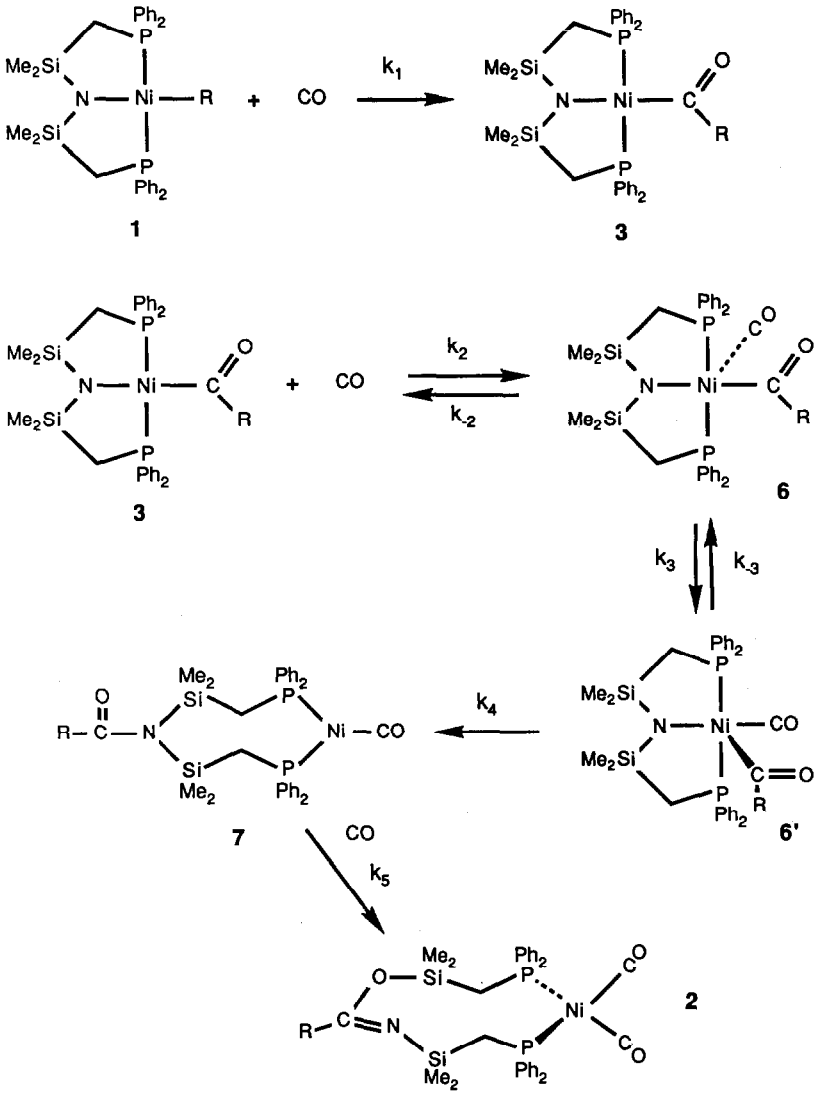

Scheme 2

carbon–oxygen and carbon–carbon bonds via reductive elimination requires the two reactive groups, especially the two hydrocarbyl ligands [3], to be *cis* disposed on the precursor nickel(II) centre for the associative mechanism to be operative. In our system, this last point is clearly not possible since the acyl and the amido ligands must be *trans*, yet the associative reductive elimination mechanism is observed. It is likely that the geometrical restrictions on C–C bond formation are lifted for C–N bond formation owing to the presence of the lone pair on the amido nitrogen. The differences in the calculated second-order rate constants for the aroylnickel complexes **3c**, **3d**, and **4** are not very significant and this precludes any discussion of substituent effects. The order of magnitude larger second-order rate constant for the vinyl derivative **1b** is notable. The fact that **1b** has the smallest hydrocarbon ligand

at nickel (vs. the more sterically demanding aroyl moiety) may be an important factor, however, in the absence of more extensive examples this is speculation.

Conclusions

The stoichiometric reductive carbonylation of amidohydrocarbylnickel(II) derivatives proceeds via the intermediacy of the corresponding acyl intermediates. No insertion of carbon monoxide into the nickel(II)–amide bond is observed. Kinetic studies are consistent with an associative pathway for the reductive elimination of the acyl and the amide groups.

Acknowledgements

Financial support was generously provided by NSERC of Canada and the Alfred P. Sloan Foundation. We thank Professor J. Trotter for the use of his X-ray diffractometer and structure solving programs, and also Professor B.R. James for helpful discussions.

References

1 M.D. Fryzuk and P.A. MacNeil, Organometallics, 1 (1982) 1540.
2 M.D. Fryzuk, P.A. MacNeil and S.J. Rettig, J. Am. Chem. Soc., 106 (1984) 6993.
3 K. Tatsumi, A. Nakamura, S. Komiya, A. Yamamoto and T. Yamamoto, J. Am. Chem. Soc., 106 (1984) 8181.
4 J.R. Norton, Acc. Chem. Res., 12 (1979) 139.
5 A.C. Balazs, K.H. Johnson, and G.M. Whitesides, Inorg. Chem., 21 (1982) 2162.
6 S.-I. Murahashi, N. Yoshimura, T. Tsumiyama, and T. Kojima, J. Am. Chem. Soc., 105 (1983) 5002.
7 (a) H.E. Bryndza, W.C. Fultz, and W. Tam, Organometallics, 4 (1985) 939; (b) C.S. Day, V.W. Day, P.J. Fagan, J.M. Manriquez, T.J. Marks, and S.H. Vollmer, J. Am. Chem. Soc., 103 (1981) 2206.
8 M.D. Fryzuk, P.A. MacNeil, S.J. Rettig, A.S. Secco, and J. Trotter, Organometallics, 1 (1982) 918.
9 L.G.L. Ward, Inorg. Synth., 13 (1972) 154.
10 M.D. Fryzuk, A. Carter, and A. Westerhaus, Inorg. Chem., 24 (1985) 642.
11 A. Seidell, Solubility of Inorganic and Metal Organic Compounds, 3rd edit., Volume 1, D. Van Nostrand Co., New York, 1940, p. 218.
12 The computer programs used include locally written programs for data processing and locally modified versions of the following: ORFLS, full-matrix least-squares, and ORFEE, function and errors, by W.R. Busing, K.O. Martin, and H.A. Levy; FORDAP, Patterson and Fourier syntheses, by A. Zalkin; ORTEP II, illustrations, by C.K. Johnson.
13 P. Coppens, L. Leiserowitz, and D. Rabinovich, Acta Crystallogr., 18 (1965) 1035.
14 J. de Meulenaer and H. Tompa, Acta Crystallogr., 19 (1965) 1014.
15 International Tables for X-ray Crystallography. Vol. VI. Kynoch Press, Birmingham, 1974.
16 T.G. Appleton, H.C. Clark, and L.E. Manzer, Coord. Chem. Rev., 10 (1973) 335.
17 (a) D.R. Fahey and J.E. Mahan, J. Am. Chem. Soc., 99 (1977) 2501; (b) M. Wada, N. Asada, and K. Oguro, Inorg. Chem., 17 (1978) 2353; (c) K. Maruyama, T. Ito, and A. Yamamoto, J. Organomet. Chem., 157 (1978) 463; (d) R. Gompper and E. Bartmann, Liebigs Ann. Chem., 2 (1980) 229; (e) G. Favero, J. Organomet. Chem., 202 (1980) 225; (f) E. Uhlig and B. Nestler, Z. Chem., 21 (1981) 451.
18 L. Pauling, The Nature of the Chemical Bond, 3rd edit., p. 224 and 252.
19 G. Huttner, O. Orama, and V. Bejenke, Chem. Ber., 109 (1976) 2533.
20 E. Carmona, F. González, M.L. Poveda, J.L. Atwood, and R.D. Rogers, J. Chem. Soc. Dalton, (1980) 2108.
21 M.F.C. Ladd and R.A. Palmer, Structure Determination by X-ray Crystallography, 2nd edit., Plenum, New York, 1985, p. 359.
22 D.R. Fahey and B.A. Baldwin, Inorg. Chim. Acta, 36 (1979) 269.
23 S. Komiya, Y. Abe, A. Yamamoto, and T. Yamamoto, Organometallics, 2 (1983) 1466.
24 S. Komiya, Y. Akai, K. Tanaka, T. Yamamoto, and A. Yamamoto, Organometallics, 4 (1985) 1130.